PRACTICAL MODELLING OF STONE-COLUMN REINFORCED GROUND

By S. A. Tan and S. Tjahyono
Assoc Prof and Research Scholar at Department of Civil Engineering,
National University of Singapore

Abstract : The acceleration of consolidation by stone columns was mostly analysed within the framework of a basic unit cell model (i.e. a cylindrical soil body around a column). A method of converting the axisymmetric unit cell into the equivalent plane-strain model would be required for two-dimensional numerical modelling of multi-column field applications. This paper proposes two practical simplified conversion methods to obtain the equivalent plane-strain model of the unit cell, and investigates their applicability to multi-column reinforced ground. In the first conversion method, the soil permeability is matched according to an analytical equation, whereas in the second method, the column width is matched based on the equivalence of column area. The validity of these methods is tested by comparison with the numerical results of unit-cell simulations and with the field data from an embankment case history. The results show that for the case of linear-elastic material modelling, both methods produce reasonably accurate long-term consolidation settlements, whereas for the case of elasto-plastic material modelling, the second method is preferable as the first one gives erroneously lower long-term settlements, where plastic yielding of stone column are ignored.

INTRODUCTION

Stone columns are commonly installed as partial replacement of soil to improve soft clay foundation for rapid embankment construction. Their main purpose is to accelerate the primary consolidation of foundation soil by means of the following two mechanisms. Firstly, the high column permeability causes radial drainage resulting in faster dissipation of excess pore water pressure, and secondly, the high column stiffness reduces foundation load or vertical stress on the soil body and so reduces the generation of excess pore water pressure. The acceleration of consolidation due to the first mechanism has been well researched, mostly in vertical drain studies where the rate of consolidation in a unit cell (i.e. a cylindrical soil body around a vertical drain) has been analytically derived with the assumption of negligible drain stiffness (Barron 1948; Hansbo 1981). This neglect of drain stiffness however may not be similarly applied to stone column studies lest it would lead to the disregard of the second mechanism and so the underestimation of the rate of consolidation. This is especially so as the high column stiffness – typically ranging from 10 to 20 times the elastic modulus of soft clay (Barksdale and Bachus 1983) – may contribute to the dissipation of pore water pressure by as much as 40% of the total dissipation by means of vertical stress reduction on the surrounding soft soil, with the rest being attributed to radial drainage (Han and Ye 2001). Han and Ye (2001) developed a simplified analytical solution for the rate of consolidation of stone-column reinforced ground that accounted for the contributions of the above two mechanisms. This solution however assumes one-dimensional deformation under loading that limit its applications to only simple cases of stone-column reinforced ground under one-dimensional compression with homogenous soil properties and regular stone-column patterns.

In vertical drain studies, several methods have been proposed to convert the axisymmetric unit cell to the equivalent plane-strain model for the purpose of two-dimensional (2D) numerical modelling of multi-drain field applications (Hird et al.1992; Indraratna and Redana 1997). These conversion methods involved the derivations of the equivalent plane-strain permeability or the equivalent plane-strain geometry based on the matching of axisymmetric and plane-strain consolidation analytical solutions. For stone-column applications, such conversion methodology needs to include a procedure for obtaining the equivalent plane-strain column stiffness so that its effect on the consolidation rate may be properly simulated in plane-strain numerical analyses. The objective of the present study is to propose simplified conversion methods to obtain the equivalent plane-strain model of the stone-column unit cell, and to investigate their applicability to multi-column reinforced ground for practical plane-strain numerical analyses.

PROPOSED CONVERSION METHODS

Based on a macroscopic approach as described in the earlier paragraph, two methods of converting the axisymmetric unit-cell model to the equivalent plane-strain model are proposed. The macroscopic approach has an advantage in permitting the formulation of simple, and yet rational, conversion methods that can be easily applied for practical geotechnical problems. These methods are described as follows.

Method 1. This method has been described in detail by Tan and Oo (2005) and is briefly reviewed here. To obtain equal flow path length normal to the column perimeter, plane-strain column (or wall) width $2b_c$ can be taken equal to the axisymmetric column diameter $2r_c$, as

shown in Fig. 1(a) and (b). This geometrical transformation has been similarly applied by Indraratna and Redana (2000) in the permeability-matching approach for the plane-strain conversion of vertical drains. In practical finite element applications, this method allows an easy transition between axisymmetric and plane-strain meshed geometry as both of them may usually be derived from the same basic (2D) input geometry. The relationship between radius of drainage zone R and its equivalent plane-strain width B (Fig. 1) may be given by the following equation based on the equivalence of total area for a square pattern of columns (Barron 1948).

$$R = 1.13B \tag{1}$$

The plane-strain material properties need to be adjusted to account for the geometrical changes. The plane-strain material stiffness is given by the following relationship based on the matching of the column-soil composite stiffness.

$$E_{c,pl} \times a_{s,pl} + E_{s,pl} \times \left(1 - a_{s,pl}\right) = E_{c,ax} \times a_{s,ax} + E_{s,ax} \times \left(1 - a_{s,ax}\right) \tag{2}$$

where E_c and E_s are elastic moduli of the column material and the surrounding soil respectively; and subscripts pl and ax denote plane-strain and axisymmetric conditions respectively. Area replacement ratio $a_s = A_c/(A_c+A_s)$, where A_c and A_s are cross-section areas of the column and the surrounding soil respectively. In this study, for simplicity, $E_{s,pl} = E_{s,ax}$, and hence $E_{c,pl}$ can be determined accordingly. The matching of the soil permeability is done using the following analytical equation as derived by Tan and Oo (2005).

$$\frac{k_{h,pl}}{k_{h,ax}} = \frac{F(N)_{pl}}{F(N)_{ax}} \left[\frac{m_{vs} m_{vc} \left(1 - a_s\right)}{m_{vc}\left(1 - a_s\right) + m_{vs} a_s} \right]_{pl} \left[\frac{m_{vc}\left(1 - a_s\right) + m_{vs} a_s}{m_{vs} m_{vc}\left(1 - a_s\right)} \right]_{ax} \frac{B^2}{R^2} \tag{3}$$

where k_h is coefficient of soil permeability in horizontal direction; $F(N) = [N^2/(N^2-1)]\ln(N)-(3N^2-1)/(4N^2)$; diameter ratio $N = R/r_c$ for axisymmetric condition, whereas $N = B/b_c$ for plane-strain condition; $m_{vs} = (\alpha_{vs})/(1+e_s)$; $m_{vc} = (\alpha_{vc})/(1+e_c)$; α_{vc} and α_{vs} are coefficients of compressibility of the column and the surrounding soil respectively; and e_c and e_s are void ratios of the columns and the surrounding soil respectively. The plane-strain coefficient of soil permeability in vertical direction $k_{v,pl}$ is expected to bear little influence on the overall consolidation rate as water flow in the soil is predominantly radial or horizontal, and is simply assumed to follow the axisymmetric value, i.e. $k_{v,pl} = k_{v,ax}$.

Method 2. An alternative geometrical transformation is based on the equivalence of the column drainage capacity in both axisymmetric and plane-strain conditions, whose concept has been proposed in a vertical drain study by Indraratna and Redana (1997) to convert vertical drain system into the equivalent plane-strain drain walls. This method hence preserves the cross-sectional areas of the column and the surrounding soil for the same total area in both conditions. The plane-strain column width is given by the following relationship based on the equivalence of area replacement ratio.

$$b_c = B \times \frac{r_c^2}{R^2} \quad (4)$$

which results in smaller plane-strain column widths and larger flow path lengths as compared to the previous method, as seen in Fig. 1(b) and (c). In practical multi-drain applications that involve high area replacement ratios (i.e. large column diameters relative to column spacing), this method may be preferable to the previous one as the enlargement (with respect to the axisymmetric geometry) of the plane-strain column area in Method 1 might result in excessively high plane-strain area replacement ratio and column drainage capacity. The plane-strain column stiffness may be similarly determined from (2), which results in equal elastic moduli for both axisymmetric and plane-strain conditions (i.e. $E_{c,pl} = E_{c,ax}$) given that $a_{s,pl} = a_{s,ax}$ and that $E_{s,pl} = E_{s,ax}$ as in the previous method. The soil permeability however cannot similarly be matched using (3) because the equation carries the assumption of equal flow path length in both axisymmetric and plane-strain conditions (Tan and Oo 2005). For simplicity, the plane-strain soil permeability is taken equal to its axisymmetric counterpart, i.e. $k_{h,pl} = k_{h,ax}$ and $k_{v,pl} = k_{v,ax}$. This method thus retains the axisymmetric material properties for the plane-strain geometry.

COMPARISON OF UNIT-CELL SIMULATIONS

To verify the proposed conversion methods, numerical simulations of unit-cell models under consolidation process have been carried out based on the axisymmetric and the equivalent plane-strain geometry. Fig. 2 shows four finite element models of a stone-column unit cell used for the simulations. The axisymmetric model is shown halved due to symmetry in Fig. 2(a), and has a height of 10 m and an outer radius of 2.550 m. The 0.850-m-radius stone column gives a diameter ratio of 3, which is within the typical range of 1.5 to 5. The model is horizontally fixed on the vertical sides and fully (i.e. horizontally and vertically) fixed on the base, and has top vertical loading which is applied through a rigid plate (Fig. 2(a)) to enforce equal vertical strain at the top boundary. For realistic simulation of unit-cell consolidation, only the top boundary is set to be pervious and the phreatic level is set at the top surface to provide pore water pressure throughout the model material. Fig. 2(b) and (c) show the equivalent plane-strain models, also halved due to symmetry, based on Methods 1 and 2 respectively. The models have an equivalent width of 2.26 m, as determined from (1), and the same boundary, phreatic, and loading conditions as the axisymmetric case. They differ in the stone-column dimension: the plane-strain-1 column width follows the axisymmetric column diameter, whereas the plane-strain-2 column width, as obtained from (4), is 0.252 m or approximately 30% of the diameter. The axisymmetric and the plane-strain models were developed using 15-node triangular elements in Plaxis 2D Version 8.0 (Brinkgreve et al. 2004). The last model in Fig 2(d) is a three-dimensional representation of a unit cell, only a quarter of which is shown due to symmetry. The model is similar to the axisymmetric case except that the geometry is rectangular instead of circular, and is similar to the plane-strain case in that they both have rectangular drainage zone. The purpose of this model is to simulate three-dimensional effects arising from the use of rectangular geometry that involves lesser degree of symmetry than the axisymmetric circular geometry. This would hence enable the measurement of potential errors resulting from the conversion of axisymmetric to rectangular geometry in the earlier plane-strain models. The widths of its square column and drainage zone are 0.753 m and 2.26 m respectively, as obtained from (1), and its

boundary, phreatic, and loading conditions follow the axisymmetric case. The model was developed using 15-node wedge elements in Plaxis 3D Tunnel Version 2 (Brinkgreve and Broere 2004).

The material parameters for the unit-cell models are presented in Table 1; where γ is unit weight; v' is Poisson's ratio in terms of effective stress for both soil and column material; c' is effective stress cohesion; φ' is effective stress angle of friction; and subscripts s and c denote soil and column material respectively. The soil type was soft clay, and the stone column was idealised as a homogenous material having certain characteristic stiffness, permeability, and strength parameters. The elastic modulus of column material is assumed to be ten times of that of soil, which is within the typical range of 10 to 20. The plane-strain-1 elastic modulus of column material is 10,980 kPa and its permeability in horizontal direction is 1.59×10^{-9} m/s, as determined from (2) and (3) respectively. The permeability of soft clay in vertical direction is assumed to be one-third of its horizontal counterpart. The strength parameters given in Table 1 correspond to the Mohr-Coulomb (MC) failure criteria, of which the effective stress cohesion is given small non-zero values to avoid numerical complications.

Simulation procedures and results

The simulation of each unit-cell model was initialised by activating instantaneous (i.e. undrained) vertical loading of 100 kPa on the top surface of the model, with equal vertical strain condition as enforced by the rigid plate (Fig. 2). The instantaneous loading implied that there was no dissipation of the generated excess pore water pressure in the model, i.e. undrained condition. This was followed by a consolidation procedure whereby dissipation of the excess pore pressure was simulated with no change in the applied loading. The dissipation was allowed to progress until the remaining excess pore pressure was very small (less than 1 kPa), at which point the simulation was ended.

Two constitutive models were considered for the representation of the unit-cell materials, giving the following two cases of simulations. In the first case (Case 1), the soil and column material were represented by the linear-isotropic-elastic model, whose behaviour was fully defined by Young's modulus and Poisson's ratio. In the second case (Case 2), the materials were idealised as the MC model with the characteristic linear-elastic-perfectly-plastic behaviour and the failure criteria defined by the strength parameters in Table 1.

The simulation results were expressed in terms of the variation of surface settlement and excess pore water pressure during the consolidation process, the latter of which was measured in soil at the base of the model geometry. Fig. 3 shows the results for Case-1 simulations with the plots following the typical consolidation trend. The initial point on each curve signifies the undrained response under the 100-kPa applied loading, which also marks the start of consolidation. The initial excess pore pressure is hence expected to be approximately 100 kPa, which is well reflected in the results except for the plane-strain-1 model. The 10% over-generation of excess pore pressure in the model may be attributed to its larger cross-sectional column area as compared with the other models, which presents higher horizontal strains in the column under both the applied loading and its own weight, and consequently larger volumetric strains in the soil elements, resulting in additional pore pressure generation in soil. The settlement curve of the

axisymmetric model is in reasonable agreement with the analytical solution of Han and Ye (2001) and the numerical solution of Balaam and Booker (1981), with the maximum differences limited to approximately 20% and 8% respectively. The settlement and excess pore pressure curves for the three-dimensional model almost match the axisymmetric case, which implies that the geometrical conversion from axisymmetry to rectangularity in the three-dimensional and the plane-strain models causes insignificant errors for this case of modelling. The results of the plane-strain-2 model also follow closely the axisymmetric case, except for slight underestimation in the settlement, of which the magnitude is limited to only 10 mm. The results of plane-strain-1 model however exhibit significant discrepancies from the norm, with as much as 30-mm and 20-kPa larger settlement and excess pore pressure respectively. The larger settlements during consolidation reflect the higher consolidation rate in the model due to its larger drainage capacity and smaller soil volume as compared with the other models. Despite these discrepancies, in period longer than 10 days – defined here as long term for convenience – the models are all in agreement with settlements of approximately 140 mm and excess pore pressure of nearly zero. This has an important implication in that the plane-strain models based on Methods 1 and 2 may both represent the axisymmetric case with reasonable accuracy for long-term settlements – often the most critical design outcome in practical applications – insofar as the linear-elastic constitutive model is used.

Fig. 4 shows the corresponding results of Case-2 simulations. Similar 10% over-generation of initial excess pore pressure is manifested by the plane-strain-1 model due to the same reason as in Case 1. The three-dimensional and the axisymmetric curves are again well matched with less than 3 mm or 6 kPa in the largest difference between them, thereby signifying that the conversion of axisymmetric to rectangular geometry yields minimal errors for Case-2 modelling. Reasonable agreement is also seen for the plane-strain-2 curves with less than 8-mm and 7-kPa underestimations in settlement and excess pore pressure respectively as compared with the axisymmetric case. As in Case-1 simulations, the plane-strain-1 model presents significant deviation from the norm with as much as 31-mm and 24-kPa larger settlement and excess pore pressure respectively in period less than a day. More importantly, its long-term settlements considerably underestimate the norm leading to a final settlement that is 22% lower than the standard magnitude of approximately 190 mm. This implies that the model may give erroneous predictions of long-term settlement when its materials are MC soils. To explain the reason for this error, the material stress state of each model at the end of the simulations is analysed and presented in Fig. 5. The axisymmetric model (Fig. 5(a)) is seen to sustain some plastic yielding in the vicinity of the column material, as indicated by the numerous plastic stress-points that are concentrated within and slightly beyond the column periphery. A plastic stress-point defines a stress state that lies on the MC failure envelope corresponding to perfectly-plastic behaviour. Similar yielding pattern, albeit with less scatter beyond the column periphery, is observed in the plane-strain-2 model (Fig. 5(c)), whereas hardly any yielding is present in plane-strain-1 model (Fig. 5(b)). This explains the different responses of the two models: the plastic yielding in the former model allows itself to simulate the settlements of axisymmetric model, whilst the latter model's elasticity gives a stiffer response leading to a lower final settlement that is indeed comparable to that in Case-1 simulations. The sustained elastic behaviour in the latter may be due to its larger cross-sectional column area with higher elastic capacity in both shearing and bending. Thus, for conditions involving plastic yielding with the MC model, the model based on

Method 1 may give incorrect representation of the axisymmetric case and so the conversion based on Method 2 is preferable.

COMPARISON WITH DATA FROM CASE HISTORY

In the second stage of verification, the proposed conversion methods were applied for the modelling of an embankment construction for Penchala Toll Plaza project at New Pantai Expressway, Malaysia, in 2003. A brief description of the project was given by Tan and Oo (2005). The embankment geometry with the stone-column reinforced soil profile is shown in Fig. 6 having a line of symmetry on the left boundary. The 20-m-wide and 1.8-m-high embankment is filled by sandy material. The stone columns, arranged in a square grid, cover a distance from the embankment base to a depth of 6 m above the layer of stiff clay. The upper crust layer is one-metre-thick fill of hard soil, which was provided as a replacement of soft-clay surface to improve ground for stable and firm construction platform as well as drainage of water during consolidation. The groundwater level is one meter below the ground surface. Two settlement plates (SP1 and SP2) as shown in Fig. 6 were installed *in situ* to measure the settlements at the centre of the embankment and at 8 m from its edge.

Three finite element models of the embankment were considered: plane-strain-1 (by Method 1), plane-strain-2 (by Method 2), and three-dimensional models. The plane-strain modelling was possible as the embankment spanned a distance of more than 200 m with approximately uniform cross-sectional geometry in the direction normal to the plane in Fig. 6. As in the unit-cell modelling, the plane-strain models were developed using 15-node triangular elements in Plaxis 2D Version 8.0, whilst the last model were formed with 15-node wedge elements in Plaxis 3D Tunnel Version 2. The widths of stone columns (or walls) in the plane-strain-1 and plane-strain-2 models were 0.80 m (i.e. equal to the actual column diameter) and 0.21 m respectively, the latter of which was obtained from (4). Owing to software limitations, the stone columns in the three-dimensional model were given equivalent rectangular geometry with square cross-sectional area, whose width was given by (1), in place of the actual circular geometry. In all models, the materials were modelled as MC soils, which were more realistic approximations of the real soils than the linear-elastic model, with parameters as listed in Table 2. The parameters are identical for all models except for the converted Young's modulus and the coefficient of soil permeability in horizontal direction for the plane-strain-1 model, whose values are determined from (2) and (3) respectively.

Simulation procedures and results

The project involved rapid embankment construction which was simulated as follows. The stone columns were first installed by partial soil replacement, following which the construction of embankment was done in three equal stages (i.e. 0.6-m increment in embankment height in each stage). These construction steps were simulated in a total of 9 days during which consolidation (i.e. dissipation of excess pore water pressure) was allowed to take place. The consolidation process was then continued with no change in loading condition until the remaining excess pore pressure fell below a specified near-zero value (1 kPa), which triggered the end of the simulation.

Fig. 7(a) and (b) show the simulated settlements at the locations of SP1 and SP2 (Fig. 6) respectively with respect to time for comparison with the measured field settlements. At both locations, the settlements of the plane-strain-2 model slightly overestimate the three-dimensional counterparts by a magnitude of less than 6 mm, or less than 9% difference, at any given time. The former model's tendency to overestimating settlements here is parallel with the results of the earlier unit-cell simulations and may imply a slight disparity in the column-soil composite stiffness in the two models. This may be attributed to the reduction in the column-soil interface area in the former model resulting from the conversion of discrete columns into plane-strain walls, which in turn causes a reduction in the total interface friction and so less stiffening effect on the soil mass. In spite of this disparity, both models predict the field data with reasonable accuracy as the deviation is limited to 15% for approximately 90% of the field data. Better agreement is seen for time greater than 60 days where the deviation is less than to 8%. On the other hand, the settlement curves for plane-strain-1 model diverge from the norm from approximately 9 days onwards and eventually reach final settlements of less than 50 mm, which grossly under-predict the field measurements of approximately 80 mm. This error is parallel with the under-prediction of long-term settlements in the unit-cell simulations using the MC model (Case 2).

The embankment settlement profiles as simulated by the plane-strain-2 and the three-dimensional models at the 20^{th} and 90^{th} days are illustrated in Fig. 8 for further comparison. The settlements are measured at the same level as SP1 and SP2 for comparison with the field measurements that are taken from the earlier graph (Fig. 7). Fig. 8 presents better similarity in the simulated and the field settlements at the 90^{th} than the 20^{th} days, reiterating an earlier finding that better agreement between the settlements is obtained in the later stages of consolidation. The settlement profiles of both models are almost identical, except for the slight deviation in the region between 5 to 15 m from the centreline where the difference is limited to only 6 mm. Small heaving is noted at distances beyond the embankment width (i.e. greater than 20 m from the centreline) as a result of stress distribution in soil around the embankment. Periodic humps in settlement profiles are also seen for distances less than about 15 m from the centreline, which correspond to the locations of the stone columns and the resulting smaller surface settlements directly above them.

Fig. 9 shows the simulated excess pore water pressure with time at the locations of A, B and C as shown in Fig. 6. At A and B, as shown by Fig. 9(a) and (b) respectively, the excess pore pressure in the models has an initial peak value of approximately 17 kPa due to the embankment construction and then dissipates with different rates to nearly zero after 100 days. Faster dissipation of excess pore pressure is seen for the plane-strain-1 model as it underestimates the results of the three-dimensional model by as much as 4 kPa during the consolidation and reaches full dissipation at shorter periods. This discrepancy is parallel with the results of the earlier unit-cell simulations and may be likewise attributed to the larger drainage capacity in the former model as compared with the others. For the plane-strain-2 model, reasonable agreement with the three-dimensional model is presented for excess pore pressure at A, whereas slight disparity manifested in as much as 2-kPa lower excess pore pressure (with respect to the latter model) is seen at B. On the other hand, at C (Fig. 9(c)), 2 m away from the embankment edge, the excess pore pressure has significantly lower peak values due to the diminished effects of the embankment loading and dissipates almost identically in all the three models, which means that

the excess pore pressure discrepancies are only confined within a distance of several metres from the stone columns. The excess pore pressure here takes much longer than 120 days to dissipate and hence the acceleration of consolidation by the stone columns is hardly evident at this location.

In order to explain the main discrepancy in the settlements of the plane-strain-1 and the plane-strain-2 models as shown in Fig. 7, the material stress state of the models at the end of consolidation are compared and presented in Fig. 10. Numerous plastic stress-points are seen in the plane-strain-2 and the three-dimensional models (Fig. 10(b) and (c)) mostly within the column periphery, signifying plastic yielding in the column material. More plastic stress-points, and so greater extent of yielding, are present in the columns near the embankment edge (or outer columns) than the inner ones. This results in larger deformation, especially the horizontal displacements, in the outer columns than the inner ones as shown in Fig. 11 for the plane-strain-2 model. The differential horizontal displacements are because the inner columns experience larger lateral restraint provided by the neighbouring columns as compared to the outer ones. This is in agreement with the experimental finding of McKelvey et al. (2004) for small groups of sand columns underneath a strip footing in soft clay. On the contrary, the column material in the plane-strain-1 model as shown in Fig. 10(c) does not yield at all and so remains elastic, which is parallel with the simulated stress state in the earlier unit-cell models and may be likewise attributed to its larger cross-sectional column area with higher elastic capacity in both shearing and bending. As a result, it gives a stiffer response with erroneously smaller settlements than the other models. This reinforces the earlier finding that Method 1 may not be correctly applied in cases involving plastic yielding, and that Method 2, which presents reasonably accurate predictions of the consolidation behaviour in the embankment case history, is the preferred conversion method.

CONCLUSION

This paper has proposed two simple conversion methods, Methods 1 and 2, to obtain the equivalent plane-strain models of stone-column reinforced ground. The main differences between the methods lie in the conversion of column geometry and the matching of soil permeability. In Method 1, the plane-strain column width is taken to be same as the actual column diameter and the soil permeability is matched according to (3); whereas in Method 2, the column width is matched according to (4) and the plane-strain soil permeability is taken to be the same as the axisymmetric case.

The validity of the methods has been tested in two stages: comparison of unit-cell simulations and comparison with the field data from an embankment case history. In the first stage, for the case of linear-elastic material modelling, both methods produce good agreement with the benchmark results of the axisymmetric and the three-dimensional models in terms of the long-term consolidation settlements, although Method 1 gives an overestimation in the consolidation rate. For the case of elasto-plastic (MC) material modelling however, Method 1 gives an erroneously lower long-term settlement as compared to Method 2 which gives good agreement with the benchmark results. The error in Method 1 has been attributed to its inability to simulate plastic yielding which occurs mostly in the column material in the process of consolidation under

loading. In the second stage where the embankment construction is simulated using the MC model, a similar discrepancy is obtained: Method 1 gives erroneously 38% lower final settlements at two measurement points as compared with the field data, whereas Method 2 presents reasonable agreement, albeit with slight deviation from the field settlements in the first 60 days of consolidation. Method 2 also achieves good agreement with the results of the three-dimensional model, despite slight disparity in the settlement curves (within 9% difference) and the excess pore pressure dissipation rate at one of the measurement points. The inaccuracy in Method 1 has been again shown to be attributed to its failure to simulate plastic yielding mainly in the column material. Thus, Method 1 would give incorrect plane-strain modelling of stone-column reinforced ground when used with elasto-plastic materials and so Method 2 is the preferred conversion method.

REFERENCES

Balaam, N. P., and Booker, J. R. (1981). "Analysis of rigid rafts supported by granular piles." *Int. J. Numer. and Analytical Methods in Geomech.*, 5, 379-403.

Barksdale, R. D., and Bachus, R. C. (1983). "Design and construction of stone columns." Federal Highway Administration, Washington D. C., FHWA/RD-83/026.

Barron, R. A. (1948). "Consolidation of fine-grained soils by drain wells." *Trans. ASCE*, 113, 718-742.

Brinkgreve, R. B. J., Broere, W. (2004). Plaxis 3D Tunnel – Version 2. Plaxis bv, Delft, The Netherlands.

Brinkgreve, R. B. J., Broere, W., and Waterman, D. (2004). Plaxis 2D – Version 8. Plaxis bv, Delft, The Netherlands.

Han, J., and Ye, S. L. (2001). "Simplified method for consolidation rate of stone column reinforced foundations." *J. Geotech. and Geoenviron. Engrg.*, ASCE, 127(7), 597-603.

Indraratna, B., and Redana, I. W. (1997). "Plane-strain modeling of smear effects associated with vertical drains." *J. Geotech. and Geoenviron. Engrg.*, ASCE, 123(5), 474-478.

Indraratna, B., and Redana, I. W. (2000). "Numerical modeling of vertical drains with smear and well resistance installed in soft clay." *Can. Geotech. J.*, 37(1), 132-145.

Hansbo, S. (1981). "Consolidation of fine-grained soils by prefabricated drains." *Proc., 10th Int. Conf. Soil Mech. and Found. Engrg.*, A. A. Balkema, Rotterdam, The Netherlands, 3, 677-682.

Hird, C. C., Pyrah, I. C., and Russell, D. (1992). "Finite element modelling of vertical drains beneath embankments on soft ground." *Geotechnique*, 42(3), 499-511.

McKelvey, D., Sivakumar, V., Bell, A., and Graham, J. (2004). "Modelling vibrated stone columns in soft clay." *Geotech. Engrg.*, 157(3), 137-149.

Tan, S. A., and Oo, K. K. (2005). "Stone column FEM modeling – 2D and 3D considerations illustrated by case history." *Proc., International Symposium on Tsunami Reconstruction with Geosynthetics*, ACSIG, Bangkok, Thailand, 157-169.

TABLE 1. Material parameters for unit-cell models

Model	γ_s (kN/m^3)	γ_c (kN/m^3)	ν'	E_s (kPa)	E_c (kPa)	$k_h \times 10^{-9}$ (m/s)	$k_v \times 10^{-9}$ (m/s)	MC parameters			
								c'_s (kPa)	φ'_s (°)	c'_c (kPa)	φ'_c (°)
Axisymmetric, plane strain 1, and three dimensional	15	20	0.3	3,000	30,000	3.47	1.16	0.1	22	1	40
Plane strain 1	15	20	0.3	3,000	10,980	1.59	1.16	0.1	22	1	40

TABLE 2. Material parameters for embankment models

Material	unsaturated γ (kN/m^3)	saturated γ (kN/m^3)	ν'	E (kPa)	k_h (m/s)	k_v (m/s)	c' (kPa)	φ' (°)
Embankment fill	18	20	0.3	15,000	1.16×10^{-5}	1.16×10^{-5}	3	33
Crust	17	18	0.3	15,000	3.47×10^{-7}	1.16×10^{-7}	3	28
Soft Clay	15	15	0.3	1,100	3.47×10^{-9}*	1.16×10^{-9}	1	20
Stiff Clay	18	20	0.3	40,000	3.47×10^{-9}	1.16×10^{-9}	3	30
Stone Column	19	20	0.3	30,000*	1.16×10^{-4}	1.16×10^{-4}	5	40

*Values are only for plane-strain-2 and three-dimensional models; correspondingly for plane-strain-1 model, E = 8,670 kPa, and $k_h = 1.68\times10^{-9}$ m/s.

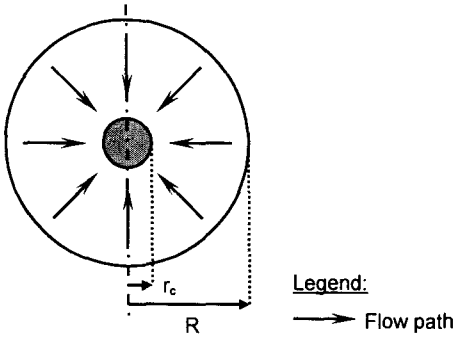

(a) Axisymmetric

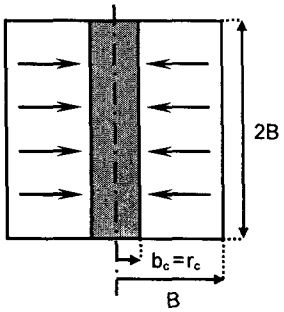

(b) Plane strain, Method 1

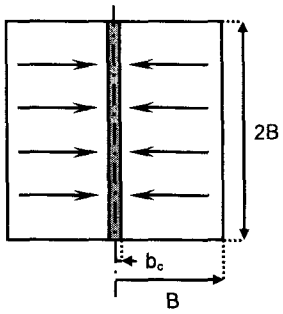

(c) Plane strain, Method 2

FIG. 1. Cross-sections of unit-cell stone column and plane-strain conversions

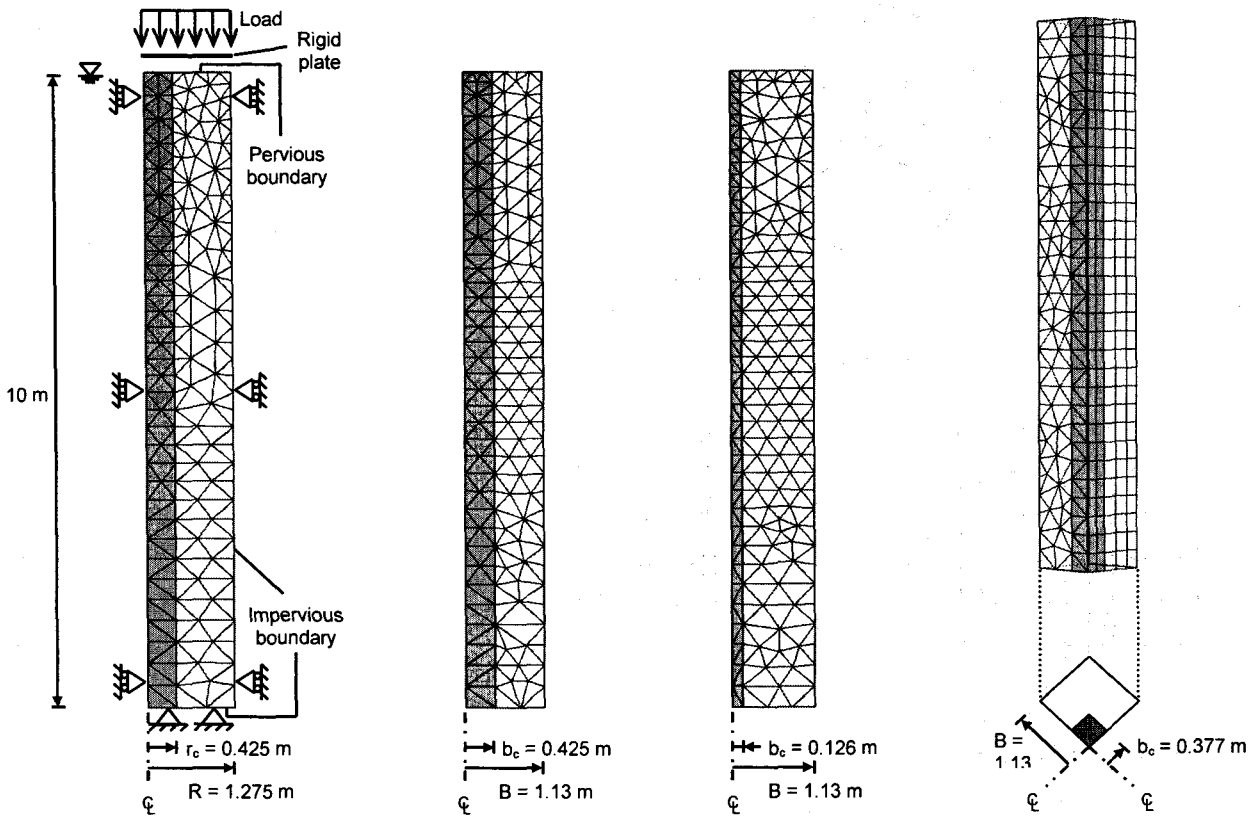

(a) Axisymmetric, with boundary and loading conditions

(b) Plane strain 1

(c) Plane strain 2

(d) Three dimensional

FIG. 2. Finite element models of a unit cell

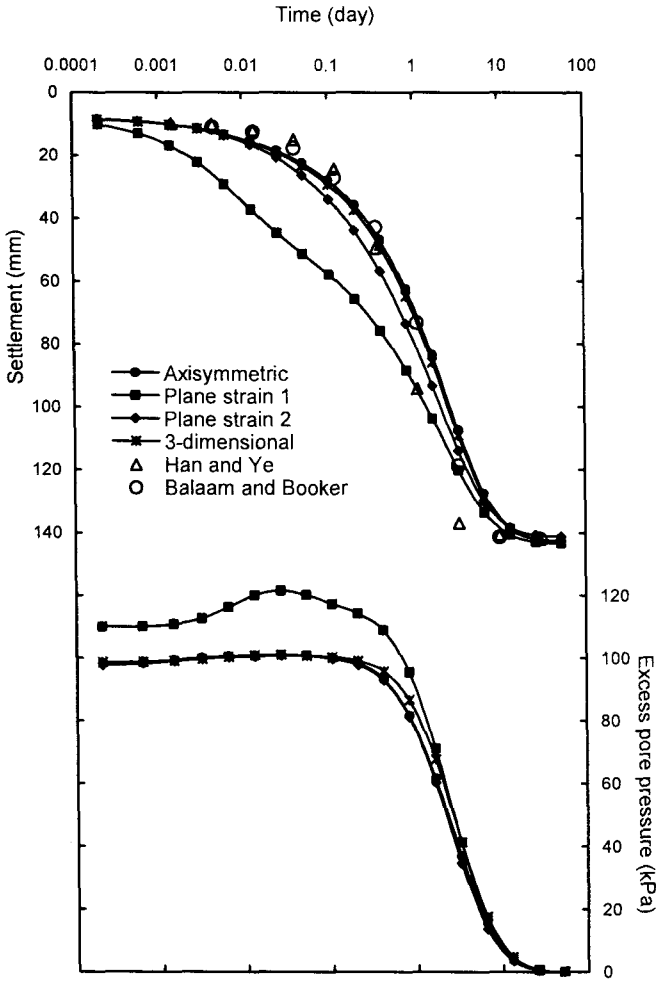

FIG. 3. Simulated unit-cell surface settlement and excess pore pressure with time for Case 1

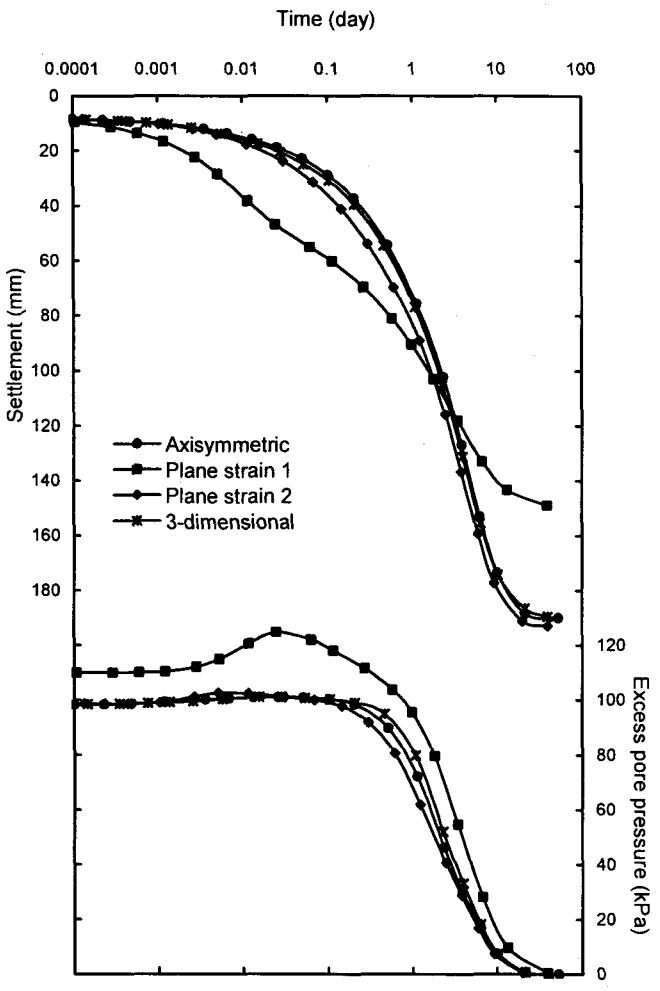

FIG. 4. Simulated unit-cell surface settlement and excess pore pressure with time for Case 2

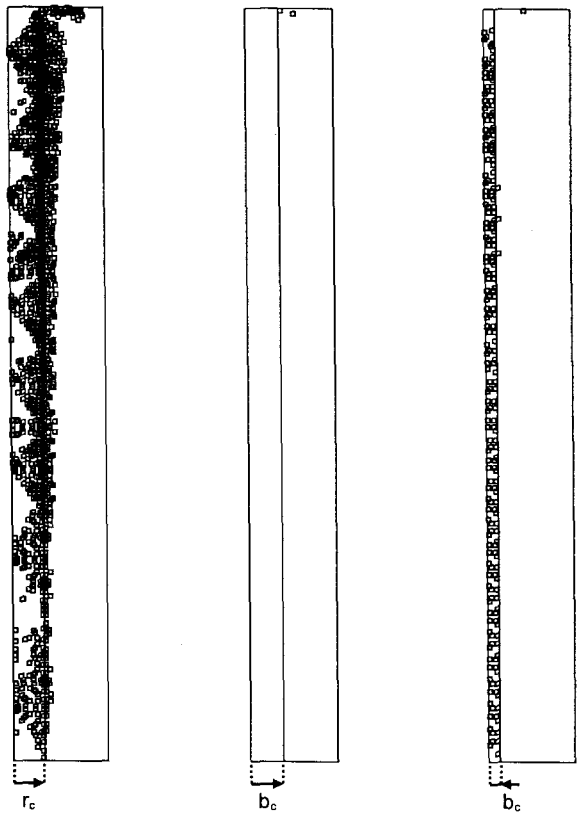

(a) Axisymmetric (b) Plane strain 1 (c) Plane strain 2

FIG. 5. Simulated plastic stress-points in unit-cell models at end of consolidation for Case 2

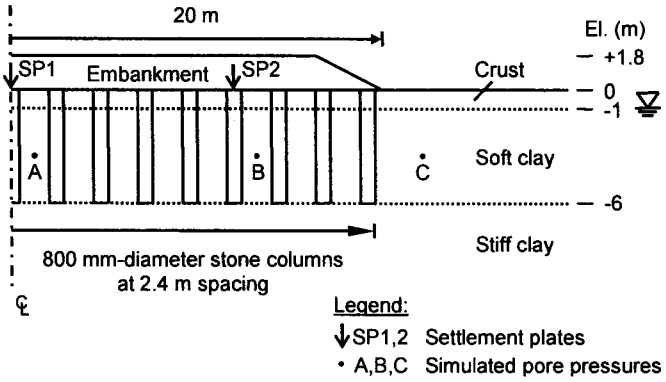

FIG. 6. Cross-section of embankment case history through centreline of stone columns

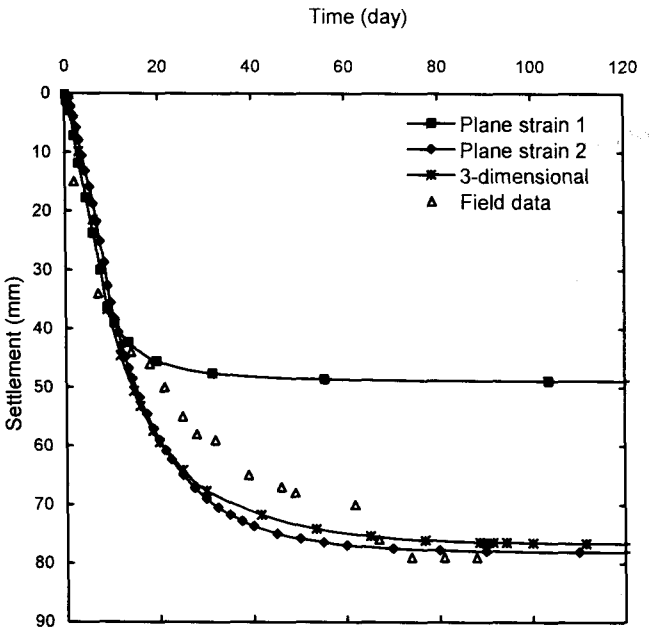

(a) Settlements at SP1

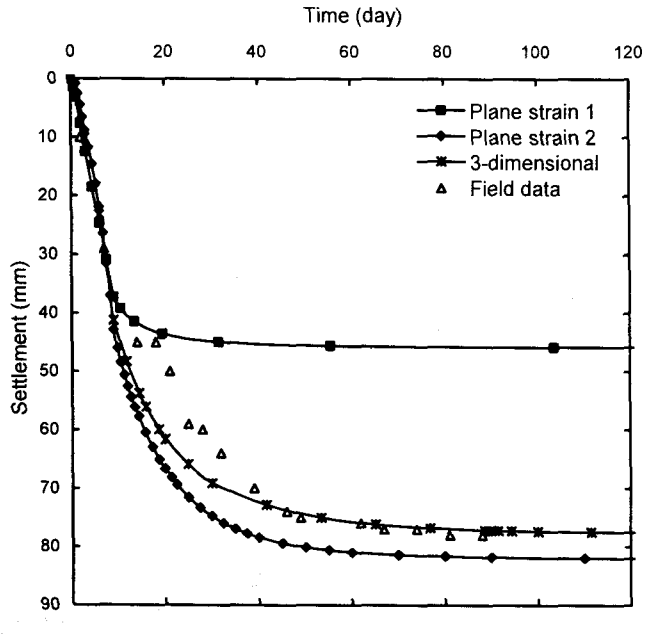

(b) Settlements at SP2

FIG. 7. Comparison between simulated and field settlements at SP1 and SP2

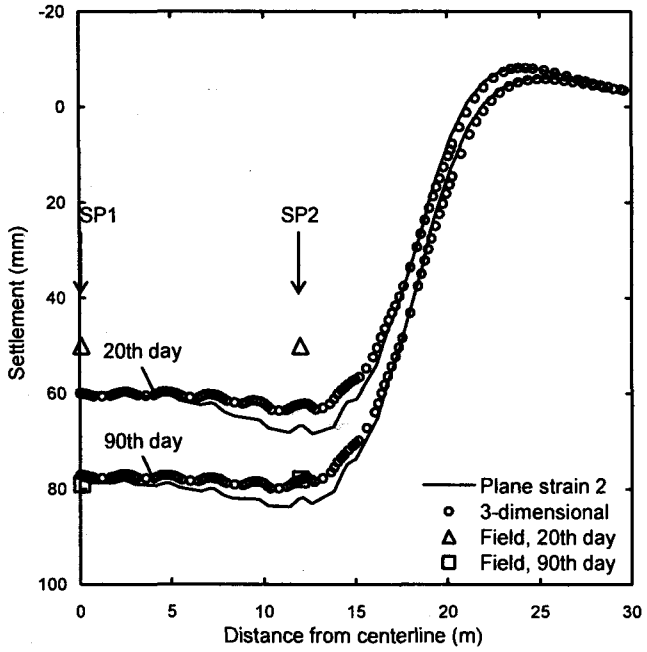

FIG. 8. Simulated embankment settlement profiles

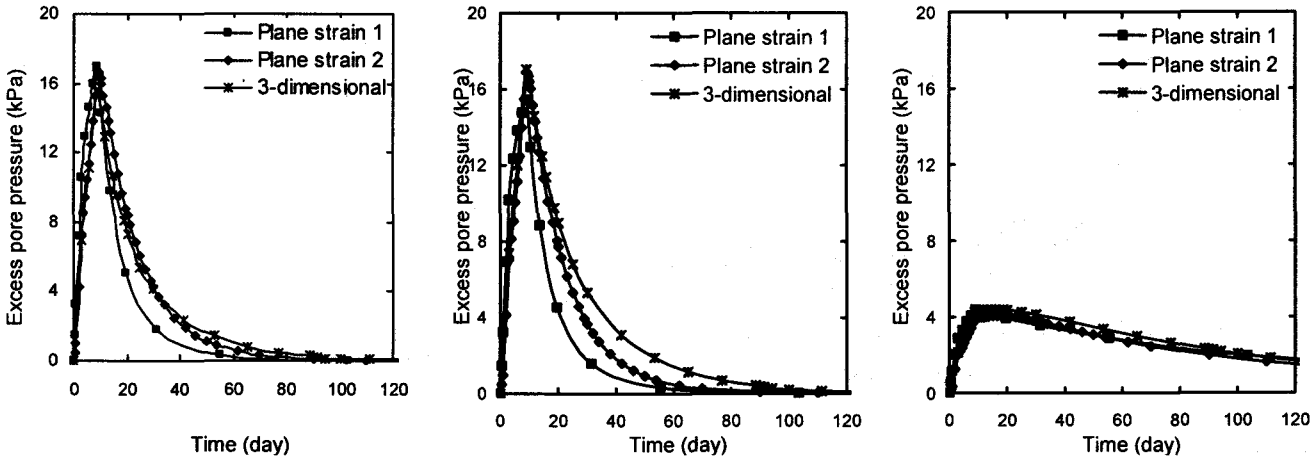

(a) Measurements at A (b) Measurements at B (c) Measurements at C

FIG. 9. Simulated excess pore pressure in embankment models

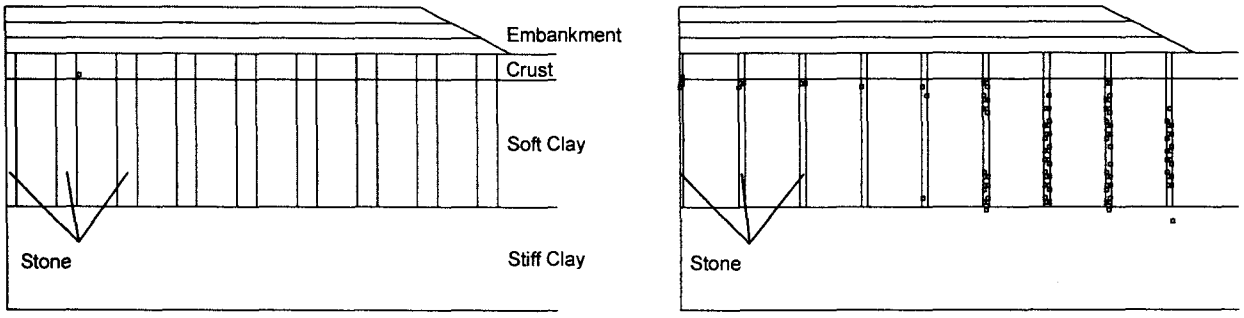

(a) Plane strain 1

(b) Plane strain 2

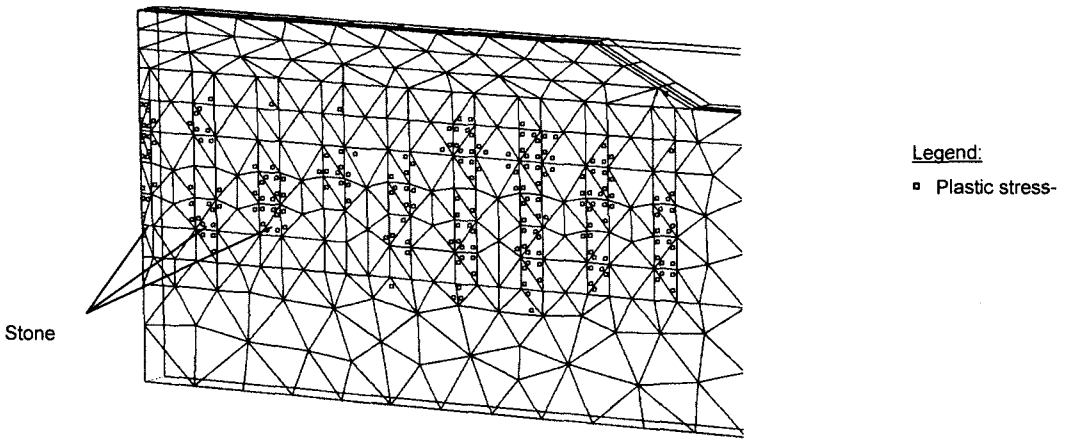

(c) Three dimensional, with mesh shown

FIG. 10. Simulated plastic stress-points in embankment models at end of consolidation

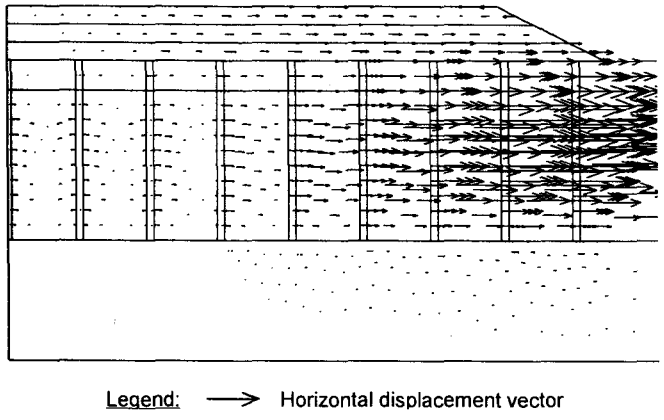

FIG. 11. Simulated horizontal displacements in plane-strain-2 model at end of consolidation